Study of Size, Shape, and Etch pit formation in InAs/InP Droplet Epitaxy Quantum Dots

Document status and date:
Published: 23/07/2022

Document Version:
Publisher's PDF, also known as Version of Record (includes final page, issue and volume numbers)

Please check the document version of this publication:

• A submitted manuscript is the version of the article upon submission and before peer-review. There can be important differences between the submitted version and the official published version of record. People interested in the research are advised to contact the author for the final version of the publication, or visit the DOI to the publisher's website.
• The final author version and the galley proof are versions of the publication after peer review.
• The final published version features the final layout of the paper including the volume, issue and page numbers.

Link to publication

PAPER • OPEN ACCESS

Study of Size, Shape, and Etch pit formation in InAs/InP Droplet Epitaxy Quantum Dots

View the article online for updates and enhancements.

Study of Size, Shape, and Etch pit formation in InAs/InP Droplet Epitaxy Quantum Dots

Raja S R Gajjela[1] , **Niels R S van Venrooij**[1]**, Adonai R da Cruz**[1] **,**
Joanna Skiba-Szymanska[2]**, R Mark Stevenson**[2]**, Andrew J Shields**[2]**,**
Craig E Pryor[3] **and Paul M Koenraad**[1]

[1] Department of Applied Physics, Eindhoven University of Technology, Eindhoven 5612 AZ, The Netherlands
[2] Toshiba Europe Limited, Cambridge Research Laboratory, 208 Science Park, Milton Road, Cambridge CB4 0GZ, United Kingdom
[3] Department of Physics and Astronomy, Optical Science and Technology Center, University of Iowa, Iowa City, Iowa IA-52242, United States of America

E-mail: r.s.r.gajjela@tue.nl

Abstract

We investigated metal-organic vapor phase epitaxy grown droplet epitaxy (DE) and Stranski–Krastanov (SK) InAs/InP quantum dots (QDs) by cross-sectional scanning tunneling microscopy (X-STM). We present an atomic-scale comparison of structural characteristics of QDs grown by both growth methods proving that the DE yields more uniform and shape-symmetric QDs. Both DE and SKQDs are found to be truncated pyramid-shaped with a large and sharp top facet. We report the formation of localized etch pits for the first time in InAs/InP DEQDs with atomic resolution. We discuss the droplet etching mechanism in detail to understand the formation of etch pits underneath the DEQDs. A summary of the effect of etch pit size and position on fine structure splitting (FSS) is provided via the $k \cdot p$ theory. Finite element (FE) simulations are performed to fit the experimental outward relaxation and lattice constant profiles of the cleaved QDs. The composition of QDs is estimated to be pure InAs obtained by combining both FE simulations and X-STM results. The preferential formation of {136} and {122} side facets was observed for the DEQDs. The formation of a DE wetting layer from As-P surface exchange is compared with the standard SKQDs wetting layer. The detailed structural characterization performed in this work provides valuable feedback for further growth optimization to obtain QDs with even lower FSS for applications in quantum technology.

Supplementary material for this article is available online

Keywords: quantum dots, X-STM, droplet epitaxy, morphology, InAs etch pits

(Some figures may appear in colour only in the online journal)

1. Introduction

III–V semiconductor quantum dots (QDs) are considered promising building blocks for quantum technologies such as quantum computing, quantum communication, and quantum information technology [1–6]. Entangled photon emission from the QDs can be generated naturally with a small fine-structure-splitting (FSS) between the exciton eigenstates. The asymmetry of QD wavefunction due to the variations in QD size, shape, strain, and composition is the main source of FSS [7]. Strain-induced formation of QDs in conventional Stranski–Krastanov (SK) growth has some limitations such as direct contact with a two-dimensional (2D) wetting layer (WL), preferential elongation of the QDs, and strain-driven intermixing of QDs all of which can strongly increase the FSS

[8, 9]. Some of the limitations of SK growth can be minimized by droplet epitaxy (DE) [10, 11] growth, which involves the splitting of group III and V fluxes, initially forming group III droplets and later crystallization of the droplets in a group V environment to form QDs.

The most important step in DE is the formation of group III droplets, which allows independent control over the size and density of the QDs. The droplet formation mainly depends on group III (In) molecular flux and the substrate temperature, which can be tuned to obtain the desired size and density of the QDs. The formed droplets are then crystallized in a group V (As) rich environment to form QDs. DEQDs formation is governed by the dissolution and adsorption of group V element by the droplet and the surrounding surface. The final shape (QDs, quantum disks, quantum rings, quantum dashes) depends on the crystallization kinetics based on group V flux and crystallization temperature [12]. Also, the formation of nanostructures is strongly influenced by the growth surface reconstruction prior to the droplet deposition [12, 13]. DE is preferable to SK growth as it provides more degrees of freedom to optimize the QDs and reduce FSS [14]. Various techniques are available to reduce FSS in QDs such as growing QDs on (111) surfaces where the underlying C_{3v} crystal symmetry assists in obtaining shape uniform QDs [15–19] and fabrication of QDs in locally etched pits to minimize anisotropy in QDs size and shape the so-called local droplet etching [20, 21]. InAs/InP self-assembled QDs emitting in the telecom range (∼1550 nm) have been developed recently with a small FSS as a result of reduced lattice mismatch and improved growth techniques [14, 22, 23]. The InAs/InP QDs have shown superior coherence in emission compared to other QD systems leading to highly indistinguishable photons [24].

The fundamental understanding of growth mechanisms (DE and SK growth) is essential for the precise tuning and optimization of QD devices for various applications. Cross-sectional scanning tunneling microscopy (X-STM) is one such technique that can probe the semiconductor QDs with atomic resolution to study not only the QDs morphology but also various effects of overgrowth such as leveling of QDs apex, intermixing, segregation, etc., [25–31]. In the current study, we investigated the morphology and composition of InAs/InP self-assembled QDs grown by both DE and SK growth by X-STM and finite element (FE) simulations. We provided an atomic-scale comparison of structural characteristics of QDs grown by both growth techniques proving that the DE is preferable in obtaining more uniform and symmetric QDs compared to SK growth [14, 24, 32, 33]. Similar samples were used to perform other experiments such as atomic force microscopy (AFM), FSS experiments, photo and electroluminescence, device fabrication, etc., and are reported elsewhere [6, 24, 33]. A detailed explanation of a partial WL formation in DEQDs is given in comparison with the standard SKWL. A mechanism of droplet etching is discussed in detail to understand the etch pit formation underneath the QDs. FE simulations are performed to fit the experimental local lattice constant and outward relaxation profiles of the cleaved QDs obtaining an estimation of QD composition. The detailed

structural analysis performed in this work provides feedback for further growth optimization of the QDs.

2. Experimental methods

As reported in [14] both DEQDs and SKQDs were grown on InP (100) substrate in a low-pressure metal-organic vapor phase epitaxy reactor with H_2 as carrier gas. For the DEQDs, the In droplets were formed on an InP buffer layer at a temperature of 400 °C in the absence of group V flux. The size and the density of the QDs can be controlled independently by optimizing the temperature and the amount of indium flux. The In droplets are then crystallized in an As-rich environment starting at a temperature of 400 °C until the substrate temperature reaches 500 °C. The DEQDs were capped with 30 nm of InP followed by excess InP at a growth temperature of 640 °C. The SKQDs were grown on an InP buffer layer at a growth temperature of 500 °C at a low growth rate of 0.05 nm s^{-1} leading to a low density of InAs QDs. The QDs were capped with 30 nm of InP at 500 °C followed by more InP at 640 °C.

All the X-STM measurements were performed in a conventional Omicron low-temperature STM at liquid nitrogen temperature (77 K) under ultra-high vacuum (UHV) 4–6×10^{-11} mbar. The measurements were carried out on a clean {110} surface freshly obtained by cleaving the sample in UHV. STM-tips were made of polycrystalline tungsten wires obtained by electrochemical etching followed by baking and Ar sputtering inside the STM preparation chamber under UHV. All the X-STM images of the QDs were acquired in constant current mode. Due to the atomic arrangement of the {110} surfaces of Zincblende crystals, only every second monolayer along the growth direction is visible in the X-STM images [34]. For filled-state imaging at high negative bias voltages, group V sublattice (P and As) was imaged, while in empty-state imaging at positive bias voltages, group III sublattice (In) was imaged. The FE simulations were performed using the structural module on COMSOL: Multiphysics and the created QD model was based on the X-STM structural characterization. A detailed explanation of FE simulations is given in section S-2 of the supplemental information (available online at stacks.iop.org/NANO/33/305705/mmedia).

3. Results and discussion

3.1. Size, shape, and composition

In figure 1, we show filled-state topographic X-STM images of DEQDs (a and b) and SKQDs (c and d) measured at a bias voltage (V_b) = −3.0 V and a tunnel current (I_t) = 50 pA. The color contrast in the image represents the relative height of the STM tip with respect to the cleaved surface. The compressively strained InAs QDs relax outward after cleaving giving rise to a bright contrast. Note that the filled-state imaging was performed at a high negative bias voltage to suppress any electronic contribution (electronic contrast) to the topography leading to a pure structural contrast [35, 36]. From figures 1(a) and (b), it is
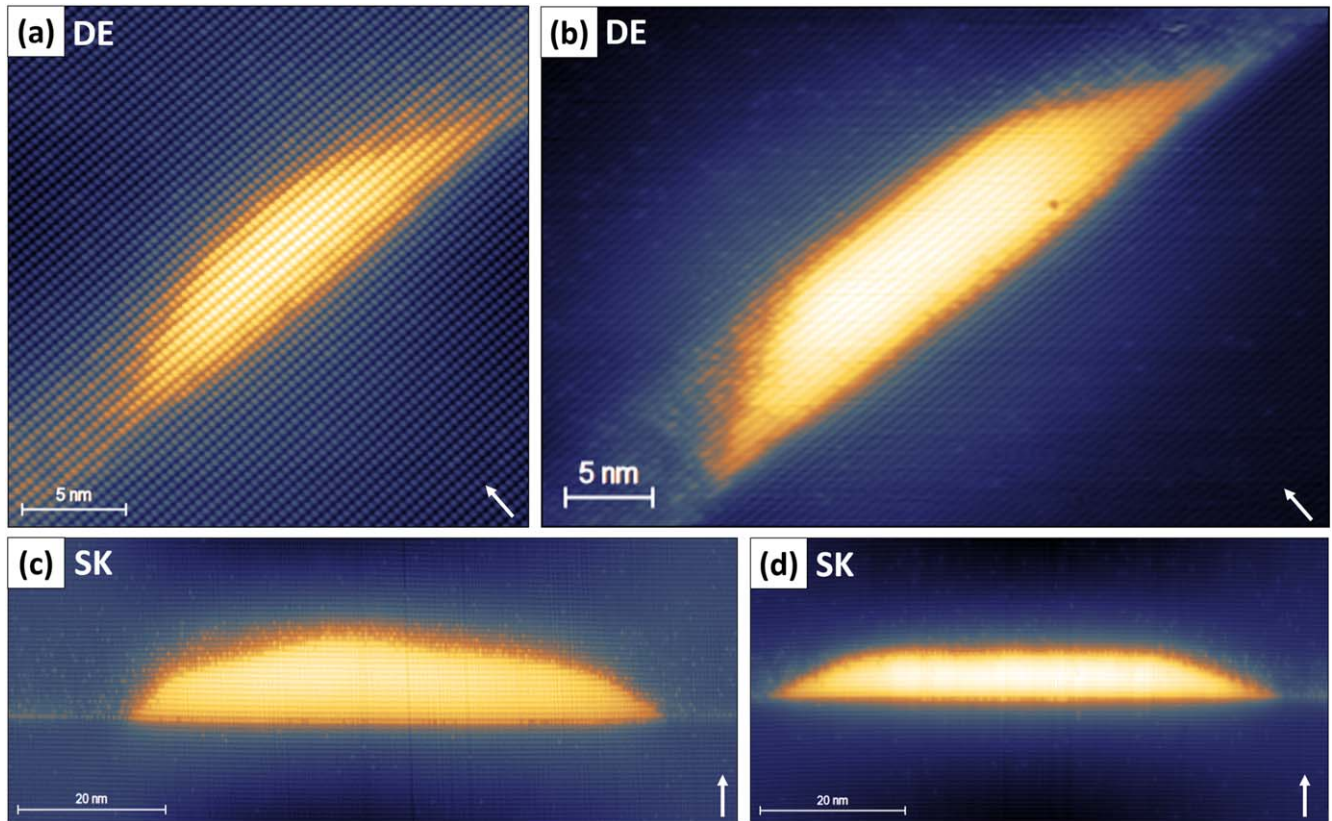
Figure 1. X-STM filled-state topographic images of InAs/InP DEQDs (a), (b) and SKQDs (c), (d) taken at bias voltage (V_b) = −3.0 V and tunnel current (I_t) = 50 pA. The dark to bright contrast represents an outward relaxation of ∼0.25 to 0.45 nm of the cleaved QDs depending on QDs size. The white arrow indicates the growth direction [100].
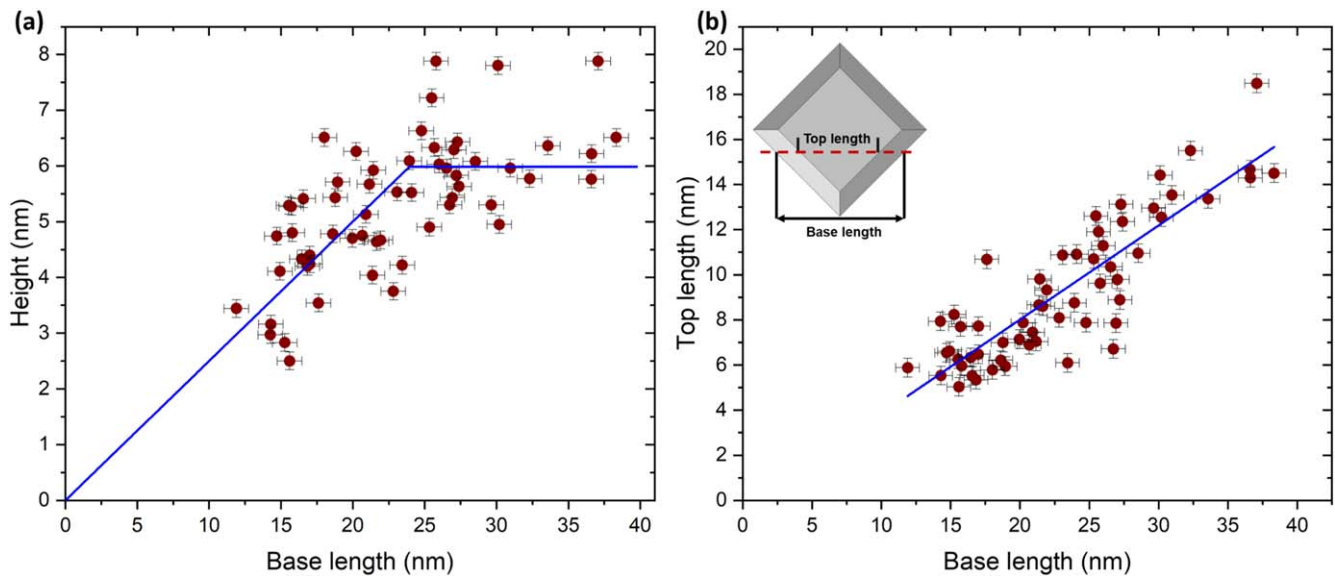
Figure 2. Height versus base length (a) and top length versus base length (b) of 58 DEQDs measured from filled-state X-STM images with a linear fit (blue) to the experimental data points. On the top corner of (b), the most probable shape of the DEQDs is given with a red line indicating the cleaving plane.

evident that the QDs are trapezoidal (truncated pyramid in 3D) shaped with (b) being the biggest DEQD found during the X-STM measurement with a base length of 38.0 ± 0.8 nm and a height of 6.5 ± 0.5 nm. All the DEQDs observed in the

experiment showed a flat top facet with a sharp interface. For the SKQD in figure 1(c), multiple side facets can be seen with the increasing height, while the SKQD in figure 1(d) is trapezoidal (truncated pyramid in 3D) shaped with a higher base

length (73.0 ± 0.8 nm for 'c' and 70.0 ± 0.8 nm for 'd') and height (11.7 ± 0.5 nm for 'c' and 7.5 ± 0.5 nm for 'd') compared to DEQDs. This is in good agreement with the AFM analysis reported in [14] for QDs grown under similar growth conditions especially the height of the DEQDs. From the AFM analysis [14], it is clear that the DEQDs appeared uniform in both directions ([110] and [1 $\bar{1}$ 0]), while the SKQDs showed a preferential elongation along [110].

The cleaving position of the sample is arbitrary and need not be through the center of every single QD, so depending on the cleaving position we observed varied heights and base lengths in the X-STM images. The relation between height and base length can be exploited to approximate the 3D size and shape of the QD. The height versus base length of all 58 DEQDs measured by X-STM is plotted in figure 2(a) with a linear fit in blue and is used to determine the orientation of the QD with respect to the cleaving plane by a simple geometrical model reported by Bruls *et al* [27, 37]. From figure 2(a), it is apparent that there is a linear relationship between the height and base length of the DEQDs and the QD height saturated at 6.0–6.5nm. Even though DEQDs are better than SKQDs in terms of size and shape uniformity, the deviation (± 1.0 nm) from the linear fit indicates a small inhomogeneity in QDs size and shape, also observed in AFM images of similar QDs [14].

As already mentioned, all the DEQDs have a flat and sharp top facet (as shown in figures 1(a) and (b)) and the length of the top facet is plotted as a function of base length in figure 2(b). The clear-cut linear dependence between top length and base length suggests that the cleaving plane is parallel to the diagonal of a near square-based truncated pyramid. The deviation from the linear fit suggests a small inhomogeneity in QDs shape. Logically, the maximum base length and top length are observed when the cleaving is through the center of the QD. As our QDs resemble model 2 from Bruls *et al* [37], the actual base length of the DEQDs is $\sqrt{2}$ times smaller than the reported diagonal base length. The absence of triangular-shaped QDs in X-STM images indicates that the top facet is very big (up to 18 nm) and flat as represented in the top left corner of figure 2(b) with a red dotted line indicating the cleaving plane. The height difference of the DEQDs observed in X-STM and AFM of similar QDs [14] is less than 1 nm. We can safely assume that the flat top facet is indeed formed before the completion of the full capping procedure and there is a little dissolution of QDs apex [38, 39]. The density of DEQDs in the sample is estimated to be 8–9×10^8 cm^{-2}. The density of SKQDs is even lower (1–2×10^8 cm^{-2}) than the density of DEQDs making it difficult to find many QDs in the X-STM measurement to provide a similar analysis for the SKQDs. However, from the AFM images of the uncapped SKQDs grown under similar conditions, it is clear that the density of SKQDs is lower and the SKQDs are elongated in [110], while the DEQDs appeared nearly uniform in both [110] and [1 $\bar{1}$ 0] [14]. The uniform contrast in figure 1 represents the uniformity in the composition of the QDs [29, 40–42]. The DEQDs in figures 1(a) and (b) show uniform contrast throughout the QDs except for some minor 'P' intermixing close to the QD edges. Conventional SKQDs show significant variation in the QDs composition [25], but we observed a uniform contrast also in

SKQDs see figures 1(c) and (d). This observation brings us to the conclusion that the composition of both DEQDs and SKQDs is close to pure InAs, which is further supported by examining the current images (shown in section S-1 of the supplemental material) of the same QDs shown in figure 1 as they are more sensitive to the local changes in composition. The change in the current response of the associated atoms and the suppressed topographic contrast makes it easy to identify alloy fluctuations within the QDs. A pure QD (e.g. InAs) gives rise to a uniform contrast in the current image.

To further support our argument on QD composition, we performed FE simulations using structural data from X-STM. The determination of the local lattice constant of the cleaved surface provides an estimation of the QD composition. Figure 3(a) shows a measured lattice constant profile of the biggest QD (shown in figure 1(b)) with a calculated lattice constant in red. Note that the lattice constant of the QD is much higher than the bulk InAs (0.60583 nm), this is due to the displacement of atomic rows upon cleaving. The outward relaxation of the cleaved QD is a function of QD size, composition, and overall strain distribution, which can be easily measured by X-STM height profiles shown in figure 3(b). The measured outward relaxation (black) of the cleaved QD is compared with the calculated relaxation profile (red) in figure 3(b). Since the X-STM images suggested pure InAs QDs, the FE simulations are performed by taking pure InAs as QD composition. A detailed explanation of FE simulations is provided in section S-2 of the supplemental material. From both figures 3(a) and (b), it is evident that the calculated lattice constant and outward relaxation profiles with a pure InAs composition fit very well with the experimental data thus, strengthening our argument that the DEQDs are indeed pure InAs. The linear elastic approximation of our FE simulations provides an effective solution but obtaining an exact solution is much more cumbersome due to the number of assumptions made in the FE simulations (refer to section S-2 of the supplemental material). We believe that this caused a small difference of ~ 20 to 30 pm between the experimental and calculated profiles, which can be seen in both figures 3(a) and (b). In general, the atomic corrugation of the surface can shift the experimental profiles in the order of 50 pm [43, 44] thus, the 20–30 pm difference is well within the acceptable range. By combining X-STM and FE simulations, it is evident that the observed DEQDs have pure InAs composition with some intermixing close to the edges. As already mentioned, due to the low density of SKQDs, the obtained structural data is limited and it is not possible to construct a reliable 3D model for FE simulations. The uniformity in topographic and current images implies that the composition of the SKQDs is also close to pure InAs, which could be a result of a lower lattice mismatch between InP and InAs compared to the InAs/GaAs system.

3.2. InAs Etch pits

The most interesting observation of the current work is the presence of etch pits underneath the DEQDs, as shown in figure 4. Almost every single QD measured by X-STM was found to be decorated with an etch pit with sizes ranging from 1
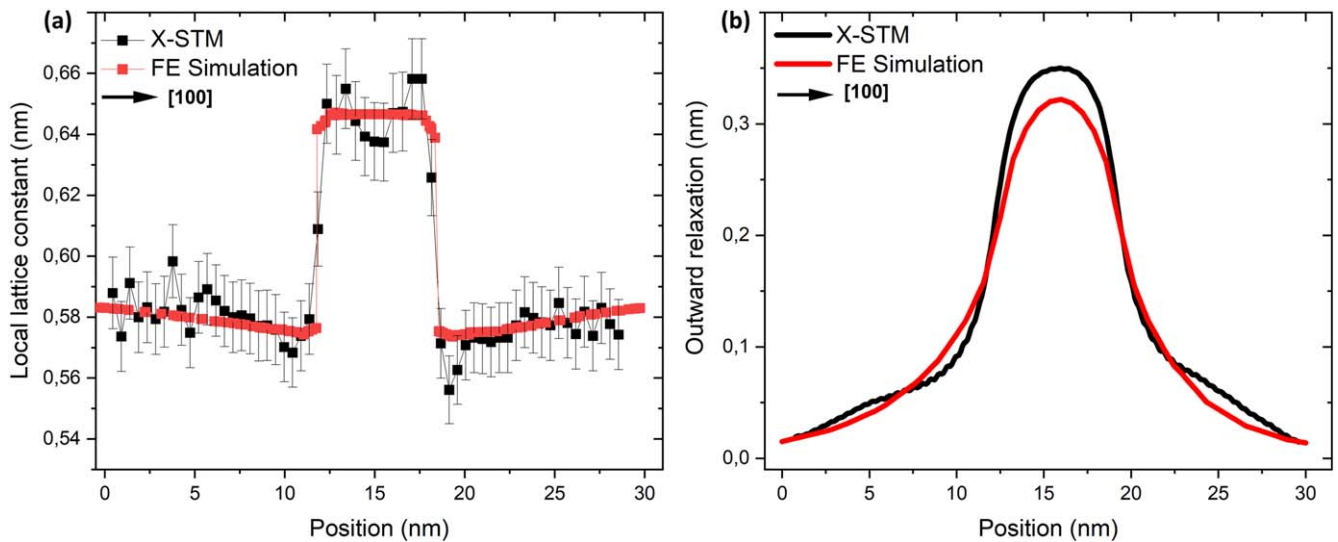
Figure 3. Local lattice constant profile (a) and STM height profile (b) of the biggest DEQD are shown in figure 1(b) as a function of position in the growth direction (from left to right). The measured lattice constant and outward relaxation is given in black with calculated profiles in red obtained via FE simulations, considering pure InAs for QD composition.
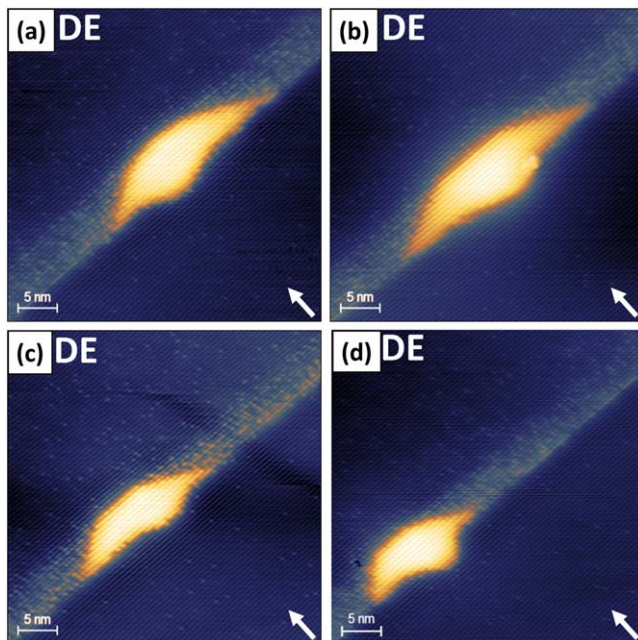

Figure 4. X-STM filled-state topographic images of the InAs etch pits in InP underneath the DEQDs with the etch pit position changing from left (a), to the center (b), and to the right (c and d) taken at $V_b = -3.0$ V and $I_t = 50$ pA. The position of the etch pit is arbitrary and the arrow indicates the growth direction [100].

bilayer (BL) to 6 BLs depending on the cleaving position. We categorize the QDs into two classes: (1) DEQDs with an etch pit of 1-2 BLs extended all over the QDs base length as shown in figures 1(a) and (b); (2) DEQDs with a deep (up to 6 BLs) and localized etch pit arbitrarily positioned underneath the QDs as shown in figure 4. Around 90% of the DEQDs found during the X-STM experiments are class 1, while the rest are class 2.

On top of that, we found an inverse correlation between the size of the etch pit and the QD. Class 1 DEQDs have a larger base length and height with a 1-2 BLs etch pit while class 2

DEQDs have a smaller height and base length with a deep ($\sim$6 BLs) and localized etch pit. This suggests that the etch pits are formed immediately after the droplet deposition. Because of the etching, the total amount of In available for the QD formation is lower for the droplets with deeper etch pits, hence smaller QDs. In figures 4(a) to (d), we show X-STM filled-state topographic images of the DEQDs with etch pits at various positions underneath QDs (from left to right). On the other hand, there is no indication of etch pit formation in SKQDs (figures 1(c) and (d), and there have never been any reports of etch pit formation in any SKQDs. Similar etch pit formation was observed for GaAs/AlGaAs DEQDs, where the mechanism of etch pit formation (local etching) was studied in detail both theoretically and experimentally [45–49]. In the GaAs/AlGaAs system, Ga droplets are formed on the AlGaAs buffer layer in the absence of As flux and the droplet liquefies the AlGaAs layer dissolving both Al and As. Due to the limited solid solubility and the concentration gradient, the As diffuses out of the droplet and crystallizes at the edges thereby etching the substrate locally. The etching rate can be controlled by growth kinetics and flux leading to a variety of nanostructures such as quantum disks and rings [12]. Even though the local droplet etching method of growing nanostructures is gaining interest as it can fabricate QDs with reduced asymmetry in QDs size and shape, the research into the In droplet etching on InP is limited [21, 22]. However, we can extrapolate a similar explanation, which was given for GaAs/AlGaAs QDs [48] to the InAs/InP system.

The reaction kinetics and the thermodynamic equilibrium between the In droplets and the InP play a crucial role in determining the etching rate and so the size of the etch pit. Considering the growth temperature of 400 °C, the phase diagram of In/InP indicates that both the liquid In and solid InP are stable phases [50]. The formed In droplets liquefies the InP buffer layer (local etching) and the P easily diffuses out of the droplet. During the crystallization, it is possible that the As can diffuse deep into the droplet and crystallize at the liquid-

solid interface giving rise to nearly pure InAs even in the etch pits [49, 51, 52]. The uniform contrast in figure 4 led us to the conclusion that the etch pits are also nearly pure InAs. However, dedicated experiments with In droplets under various growth conditions are required to improve the fundamental understanding of the etching mechanism in In/InP system which is outside the scope of this work. It can be seen from figure 4 that there is an InP(As) layer matching the height of the QD with a tiny amount (a few percent) of As. During the capping of the QDs, the incoming P can drive As from the QD apex to the sides forming a dilute InP(As) layer close to the QD. The thickness of this layer matches the QD height and we observed that when we move away from the QD, this InP(As) layer disappears quickly within 10 nm from the QD.

Shape asymmetry of the QDs due to the presence of localized etch pits can strongly influence the FSS of the QDs. For this reason, we performed a detailed analysis of the effect of etch pit size and position on the FSS. In this analysis, the excitonic configuration of several QD geometries was simulated numerically. $k \cdot p$ envelope function theory [53–55] was used to obtain the single-particle electron and hole QD states. The single-particle states were then combined in a configuration interaction calculation to compute the different exciton energy levels. The detailed results will be presented in a future dedicated theoretical article, however here we report some major observations. We considered two situations to assess the effect of etch pit size and position. First, we fixed the position of the etch pit and increased the base length of the etch pit. Second, the size of the etch pit was kept constant while the etch pit position was shifted along the diagonal axis. The increase of the base length appeared to *reduce* the FSS approximately by a factor of 2 for an etch pit base length as big as the QD. This is mainly due to the reduction in the overlap between the electron and hole wavefunction due to the leakage of both single-particle states into the etch pit region. On the other hand, shifting the position of the etch pit *increased* the FSS by almost 40 times compared to the situation in which the same etch pit is centered. Therefore, a QD with a perfectly centered etch pit has lower FSS when compared to a QD with an off-centered etch pit. As controlling the etch pit position is not possible via conventional growth, the class 1 QDs appear to be the logical choice to obtain QDs with lower FSS.

3.3. QD side facets

Another notable observation from our X-STM experiments on DEQDs is the orientation of QD side facets with respect to the base plane (100). We determined the side facet miller indices of the QDs by measuring the angle between the side facets and the base plane, as shown in figure 5, where the left facet is at an angle of $47.7° \pm 2°$ while the right facet is found to be at an angle of $28.2° \pm 2°$. In figure 5 we color-coded the side facets based on the facet angle, where black represents the base plane (100), green represents one of the {122} planes, and pink represents one of the {136} planes. Michon *et al* [56] performed a detailed thermodynamic analysis of QDs size and shape showing the formation of {136} side facets for the InAs/InP QDs. The same {136} facets were also observed for (InGa)
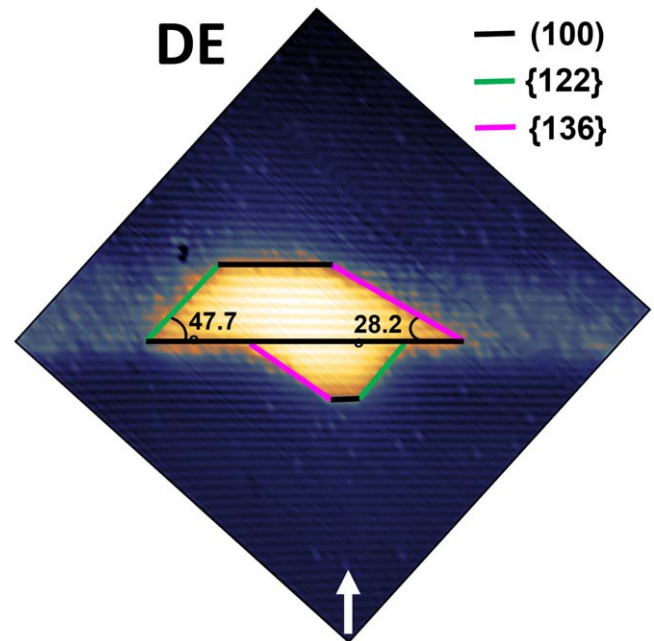

Figure 5. X-STM image showing the side facets of QDs along with faceted etch pit. The different colors represent: black (100) plane; green {122} plane; pink {136} plane. The white arrow indicates the growth direction [100]. X-STM image shown here has been taken from the [28] and modified to show the side facet angles with the base plane (100). Reproduced from [28]. CC BY 4.0.
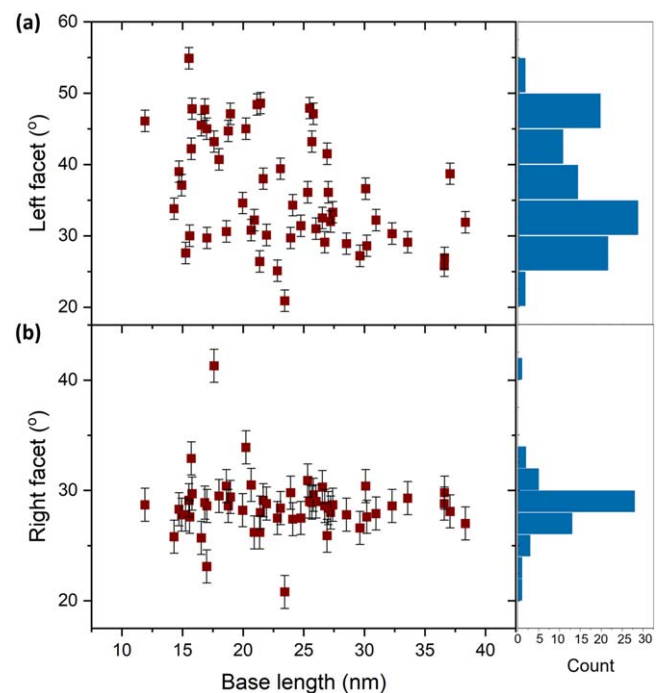

Figure 6. The angle of the left (a) and right (b) facets of the DEQDs with respect to the base plane (100) as a function of base length measured by X-STM. On the right, a frequency plot is shown to observe the distribution of facet angles.

As QDs in GaP reported by Robert *et al* [57, 58]. Another interesting observation is that the etch pit appeared to have mirror symmetry with the side facets of the QD, as shown in figure 5. The left facet of the etch pit is parallel to the {136}
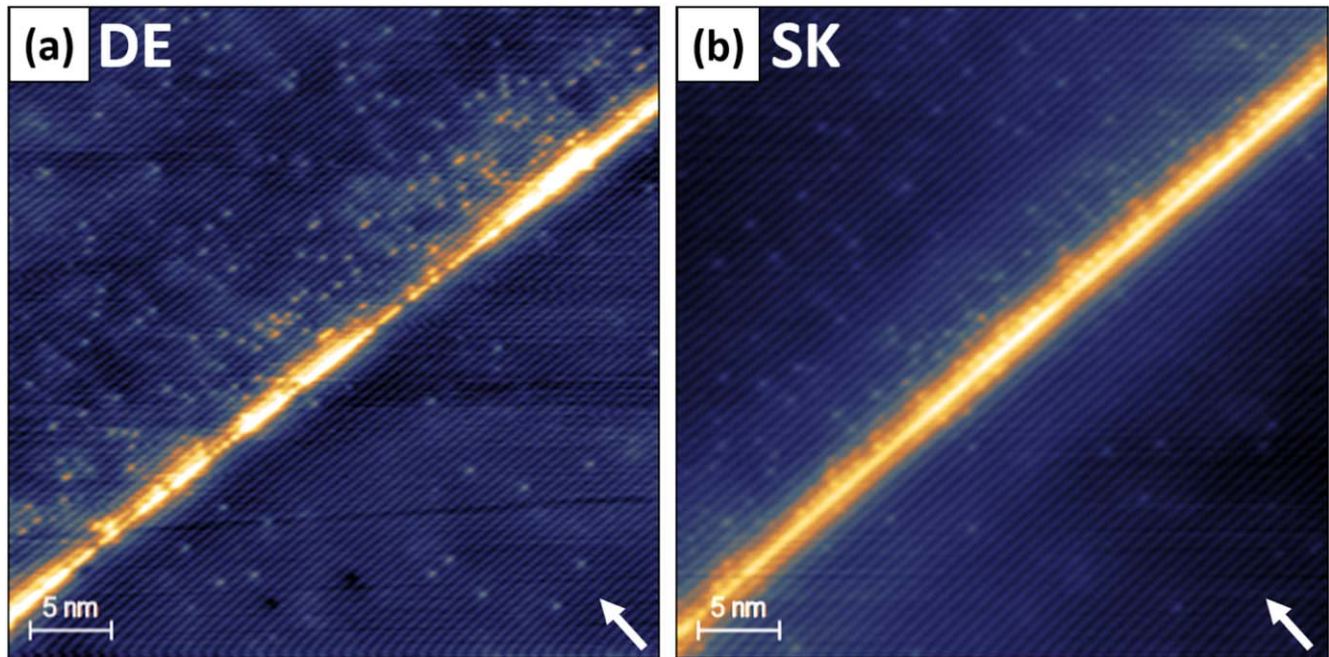
Figure 7. X-STM filled-state topographic images of the wetting layer in DEQDs (a) and SKQDs (b) taken at $V_b = -3.0$ V and $I_t = 50$ pA present a clear difference from one another. The arrow indicates the growth direction [100].

plane and the right facet is parallel to the {122} plane. We also identified a small (100) plane at the bottom of the etch pit.

We measured the facet angles of all the DEQDs found during the X-STM measurement. In figure 6, we show the measured angles of the left facet (a) and right facet (b) as a function of base length along with their distribution. It is clear from figure 6(a) that the left facet has two preferable facets one making $28° \pm 2°$ ({136} plane) and the other $47° \pm 2°$ ({122} plane) with the base plane (100). The trend is clearly visible in the frequency plot given on the right side of figure 6(a). On the other hand, the right facet of almost all the DEQDs has a {136} plane making an angle of $28° \pm 2°$ with a (100) base plane. On whole, around 70% of the measured DEQDs have {136} planes for both left and right facets. The final facets of the QD are strongly dependent on the reaction kinetics at the growth front leading to the same or different side facets on all QD sides. The provided indices for the side facets are purely based on the angle between side facets and the base plane (100). It is a rudimentary observation and *in situ* surface STM measurements are necessary to confirm this observation. Also, measurements on samples with different growth conditions and a study of growth kinetics are needed to provide a detailed explanation for the formation of different QD facets, both are outside the scope of this work. However, the increased asymmetry of QDs due to the different side facets might contribute to a further increase in the FSS.

3.4. DE versus SK wetting layer

In SKQDs, it is impossible to form QDs without a WL, on the other hand, there is no such constraint in DEQDs. We now shift our focus to the X-STM observation of WL formation in both DE and SKQDs. Figure 7 shows the X-STM filled-state topographic images of the DEWL (a) and SKWL (b). We

observed a discontinuous layer of InAs(P) for DEWL as shown in figure 7(a). The estimated composition of the WL is $InAs_xP_{1-x}$, where $x = {\sim}0.65$ was obtained via the atom counting method [59] and also by comparing the outward relaxation profiles of the DE and SKWLs as shown in figure 8. The discontinuity in the DEWL is clearly visible in the X-STM image. The discontinuous WL formation is associated with the As-P exchange at the growth surface [60–62]. It is well-known that the As can easily replace P during the arsenization of the In droplets [60]. As we can see from figure 7(b), the SKWL is a standard continuous 2D layer with a thickness of 1-2 BLs and pure InAs in composition. By growing QDs in DE mode, we can avoid the formation of a 2D WL that undermines the 3D confinement of charge carriers in the QDs. Based on the X-STM analysis of the WL, the growth conditions can be further optimized to suppress the As-P exchange at the growth surface.

STM height profiles of both DEWL and SKWL are shown in figure 8 as a function of position in the growth direction. As mentioned earlier the SKWL is a standard 2D WL whereas the DEWL is a discontinuous layer with As-rich regions. The outward relaxation of the cleaved surface strongly depends on the composition of the grown layers. In figure 8, the STM height profile taken at an As rich (DEWL1) and As poor (DEWL2) region is shown in comparison with an SKWL. It is obvious that the SKWL with pure InAs relaxed higher (${\sim}0.11$ nm) than the discontinuous DEWL (${\sim}0.08$ nm) further supporting our observations on WL formation. The formation of a discontinuous WL might be analogous to the formation of In rich islands in InAs submonolayer QD growth [59, 63], where the ML high In rich islands are formed and are stacked to form a QD [64]. In the DE case, there is an excess In on the surface after droplet formation as the surface
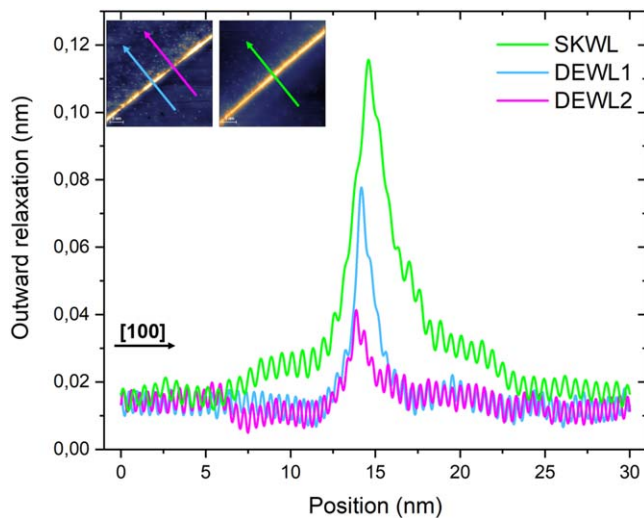
Figure 8. The STM height profile of the DEWL and SKWL as a function of position in the growth direction. On the top left corner, images from figure 7 are given with arrows indicating the position and direction of the STM height profiles. The black arrow indicates the growth direction [100].

is In terminated. Once the epitaxial surface is exposed to AsH_3 to allow the crystallization of the In droplets, the excess In on the InP surface can react with As to form InAs rich regions along with the As-P surface exchange, forming a discontinuous layer of InAs(P). The composition and thickness of these InAs(P) depend on the AsH_3 flow, growth temperature, and exposure time. The formation of the InAs(P) layer can be minimized by controlling the growth parameters or by growing an interlayer (such as lattice-matched InGaAs) [23] to avoid the surface As-P exchange.

4. Conclusions

In summary, we investigated and compared the structural characteristics of InAs/InP DE and SKQDs through atomic-resolution X-STM analysis. We showed that the DEQDs have better uniformity in terms of QDs size and shape compared to conventional SKQDs. X-STM (both topographic and current) images in conjunction with FE simulations, obtained pure InAs for QDs composition with very little intermixing close to the edges of the QDs. We found that the In droplets drill into underlying InP via a local etching process forming localized etch pits. During the crystallization, the As can diffuse all the way into the etch pit providing a pure InAs composition for the etch pits. A summary of the effect of etch pit size and position on FSS obtained via the $k \cdot p$ theory was presented. According to the calculations, a QD with a perfectly centered etch pit has lower FSS than a QD with an off-centered etch pit. We showed that the InAs/InP DEQDs have preferential {136} planes for both left and the right facets of the QDs with occasional {122} for the left facet. We observed a partial WL for DEQDs due to the surface As-P exchange, while the SKQDs have a standard 2D WL with a thickness of 1 BL. Overall, the structural analysis presented in this work uncovers not only the morphology and composition of the

QDs but also the presence of etch pits underneath the DEQDs providing valuable feedback to the growers for further growth optimization of the QDs to reduce the fine structure splitting.

Data availability statement

The data that support the findings of this study are available upon reasonable request from the authors.

Author contributions

R.S.R.G, J.S-S, and P.M.K conceived the original idea for this work. R.S.R.G and P.M.K performed X-STM experiments, FE simulations, and the related analysis. N.R.S.V, A.R.da.C, and C.E.P performed the theoretical calculations on the effect of etch pit on FSS of QDs with an etch pit. J.S-S., R.M.S, and A. J.S were involved in the analysis, discussion, and interpretation of the results. R.S.R.G wrote the manuscript where all the authors contributed to the overall scientific interpretation and editing of the manuscript. P.M.K supervised the whole work.

Conflict of interest

The authors declare no conflicts of interest.

ORCID iDs

Raja S R Gajjela ● https://orcid.org/0000-0003-2328-2883
Adonai R da Cruz ● https://orcid.org/0000-0001-8719-399X
Craig E Pryor ● https://orcid.org/0000-0002-4351-3688
Paul M Koenraad ● https://orcid.org/0000-0002-3813-1474

References

[1] Hadfield R H 2009 *Nat. Photonics* **3** 696
[2] Li X 2003 *Science* **301** 809
[3] Nilsson J *et al* 2013 *Nat. Photonics* **7** 311

[4] Varnava C, Stevenson R M, Nilsson J, Skiba-Szymanska J, Dzurňák B, Lucamarini M, Penty R V, Farrer I, Ritchie D A and Shields A J 2016 *Npj Quantum Inf.* **2** 16006

[5] Huwer J, Stevenson R M, Skiba-Szymanska J, Ward M B, Shields A J, Felle M, Farrer I, Ritchie D A and Penty R V 2017 *P. Rev. Appl.* **8** 024007

[6] Stevenson R M, Young R J, Atkinson P, Cooper K, Ritchie D A and Shields A J 2006 *Nature* **439** 179

[7] Gammon D, Snow E S, Shanabrook B V, Katzer D S and Park D 1996 *Phys. Rev. Lett.* **76** 3005

[8] Finley J J, Mowbray D J, Skolnick M S, Ashmore A D, Baker C, Monte A F G and Hopkinson M 2002 *Phys. Rev. B* **66** 153316

[9] Tartakovskii A I *et al* 2004 *Phys. Rev.* B **70** 193303

[10] Koguchi N, Takahashi S and Chikyow T 1991 *J. Cryst. Growth* **111** 688

[11] Gurioli M, Wang Z, Rastelli A, Kuroda T and Sanguinetti S 2019 *Nat. Mater.* **18** 799

[12] Somaschini C, Bietti S, Koguchi N and Sanguinetti S 2009 *Nano Lett.* **9** 3419

[13] Koguchi N and Ishige K 1993 *Japan. J. Appl. Phys.* **32** 2052

[14] Skiba-Szymanska J *et al* 2017 *Phys. Rev. Appl.* **8** 014013

[15] Kuroda T *et al* 2013 *Phys. Rev.* B **88** 041306

[16] Liu X, Ha N, Nakajima H, Mano T, Kuroda T, Urbaszek B, Kumano H, Suemune I, Sakuma Y and Sakoda K 2014 *Phys. Rev.* B **90** 081301

[17] Bietti S, Basset F B, Tuktamyshev A, Bonera E, Fedorov A and Sanguinetti S 2020 *Sci. Rep.* **10** 6532

[18] Tuktamyshev A, Fedorov A, Bietti S, Tsukamoto S and Sanguinetti S 2019 *Sci. Rep.* **9** 14520

[19] Bietti S, Esposito L, Fedorov A, Ballabio A, Martinelli A and Sanguinetti S 2015 *Nanoscale Res. Lett.* **10** 247

[20] Huo Y H, Rastelli A and Schmidt O G 2013 *Appl. Phys. Lett.* **102** 152105

[21] Sala E M, Na Y I, Godsland M, Trapalis A and Heffernan J 2020 *Phys. Status Solidi (RRL)* **14** 2000173

[22] Sala E M, Godsland M, Trapalis A and Heffernan J 2021 *Phys. Status Solidi (RRL)* **14** 2100283

[23] Sala E M, Godsland M, Na Y I, Trapalis A and Heffernan J 2021 *Nanotechnology* **33** 065601

[24] Anderson M, Müller T, Skiba-Szymanska J, Krysa A B, Huwer J, Stevenson R M, Heffernan J, Ritchie D A and Shields A J 2021 *Appl. Phys. Lett.* **118** 014003

[25] Offermans P, Koenraad P M, Wolter J H, Pierz K, Roy M and Maksym P A 2005 *Phys. Rev.* B **72** 165332

[26] Gong Q, Nötzel R, Hamhuis G J, Eijkemans T J and Wolter J H 2002 *Appl. Phys. Lett.* **81** 1887

[27] Bruls D, Vugs J, Koenraad P, Skolnick M, Hopkinson M and Wolter J 2001 *Appl. Phys. A* **72** S205

[28] Gajjela R S R and Koenraad P M 2021 *Nanomaterials* **11** 85

[29] Offermans P, Koenraad P M, Wolter J H, Song J D, Kim J M, Bae S J and Lee Y T 2003 *Appl. Phys. Lett.* **82** 1191

[30] Çelebi C, Ulloa J M, Koenraad P M, Simon A, Letoublon A and Bertru N 2006 *Appl. Phys. Lett.* **89** 023119

[31] Gajjela R S R, Hendriks A L, Douglas J O, Sala E M, Steindl P, Klenovský P, Bagot P A J, Moody M P, Bimberg D and Koenraad P M 2021 *Light: Sci. Appl.* **10** 125

[32] Anderson M, Müller T, Skiba-Szymanska J, Krysa A B, Huwer J, Stevenson R M, Heffernan J, Ritchie D A and Shields A J 2020 *Phys. Rev. Appl.* **13** 054052

[33] Müller T, Skiba-Szymanska J, Krysa A B, Huwer J, Felle M, Anderson M, Stevenson R M, Heffernan J, Ritchie D A and Shields A J 2018 *Nat. Commun.* **9** 862

[34] Feenstra R M, Stroscio J A, Tersoff J and Fein A P 1987 *Phys. Rev. Lett.* **58** 1192

[35] Feenstra R 1999 *Physica* B **273-274** 796

[36] Feenstra R M 1994 *Semicond. Sci. Technol.* **9** 2157

[37] Bruls D M, Vugs J W A M, Koenraad P M, Salemink H W M, Wolter J H, Hopkinson M, Skolnick M S, Long F and Gill S P A 2002 *Appl. Phys. Lett.* **81** 1708

[38] Utrilla A D *et al* 2018 *Appl. Surf. Sci.* **444** 260

[39] Gong Q, Offermans P, Nötzel R, Koenraad P M and Wolter J H 2004 *Appl. Phys. Lett.* **85** 5697

[40] Giddings A D, Keizer J G, Hara M, Hamhuis G J, Yuasa H, Fukuzawa H and Koenraad P M 2011 *Phys. Rev. B* **83** 205308

[41] Bocquel J, Giddings A D, Mano T, Prosa T J, Larson D J and Koenraad P M 2014 *Appl. Phys. Lett.* **105** 153102

[42] Offermans P, Koenraad P M, Nötzel R, Wolter J H and Pierz K 2005 *Appl. Phys. Lett.* **87** 111903

[43] Davies J H, Bruls D M, Vugs J W A M and Koenraad P M 2002 *J. Appl. Phys.* **91** 4171

[44] Davies J H, Offermans P and Koenraad P M 2005 *J. Appl. Phys.* **98** 053504

[45] Zocher M, Heyn C and Hansen W 2019 *J. Appl. Phys.* **125** 025306

[46] Li X, Wu J, Wang Z M, Liang B, Lee J, Kim E-S and Salamo G J 2014 *Nanoscale* **6** 2675

[47] Heyn C, Stemmann A and Hansen W 2009 *Appl. Phys. Lett.* **95** 173110

[48] Heyn C 2011 *Phys. Rev.* B **83** 165302

[49] Wang Z M, Liang B L, Sablon K A and Salamo G J 2007 *Appl. Phys. Lett.* **90** 113120

[50] Ansara I *et al* 1994 *Calphad* **18** 177

[51] Stemmann A, Heyn C, Köppen T, Kipp T and Hansen W 2008 *Appl. Phys. Lett.* **93** 123108

[52] Keizer J G 2012 Atomic-scale probing of metallic and semiconductor nanostructures *Ph D Thesis* Technische Universiteit Eindhoven

[53] Pryor C E and Pistol M-E 2015 *J. Appl. Phys.* **118** 225702

[54] Pryor C 1998 *Phys. Rev.* B **57** 7190

[55] Landin L, Pistol M-E, Pryor C, Persson M, Samuelson L and Miller M 1999 *Phys. Rev.* B **60** 16640

[56] Michon A, Sagnes I, Patriarche G, Beaudoin G, Mérat-Combes M N and Saint-Girons G 2006 *Phys. Rev.* B **73** 165321

[57] Robert C *et al* 2012 *Phys. Rev.* B **86** 205316

[58] Robert C *et al* 2016 *Phys. Rev.* B **94** 075445

[59] Gajjela R S R, Hendriks A L, Alzeidan A, Cantalice T F, Quivy A A and Koenraad P M 2020 *Phys. Rev. Mater.* **4** 114601

[60] Yoon S, Moon Y, Lee T W, Yoon E and Kim Y D 1999 *Appl. Phys. Lett.* **74** 2029

[61] Yang H, Ballet P and Salamo G J 2001 *J. Appl. Phys.* **89** 7871

[62] Gutiérrez H R, Cotta M A, Bortoleto J R R and de Carvalho M M G 2002 *J. Appl. Phys.* **92** 7523

[63] Alzeidan A, Cantalice T, Vallejo K, Gajjela R, Hendriks A, Simmonds P, Koenraad P and Quivy A 2022 *Sensors Actuators* A **334** 113357

[64] Leonard D, Krishnamurthy M, Reaves C M, Denbaars S P and Petroff P M 1993 *Appl. Phys. Lett.* **63** 3203